Remote Sensing of Environment 115 (2011) 130–142

Contents lists available at ScienceDirect

Remote Sensing of Environment

journal homepage: www.elsevier.com/locate/rse

Sub-pixel precision image matching for measuring surface displacements on mass movements using normalized cross-correlation

Misganu Debella-Gilo *, Andreas Kääb

Institute of Geosciences, University of Oslo, P. O. Box 1047, Oslo, Norway

ARTICLE INFO

Article history:
Received 10 February 2010
Received in revised form 18 August 2010
Accepted 19 August 2010

Keywords:
Normalised cross-correlation
Sub-pixel precision
Image matching
Displacement measurement
Rockglacier
Glacier
Rock slide

ABSTRACT

This study evaluates the performance of two fundamentally different approaches to achieve sub-pixel precision of normalised cross-correlation when measuring surface displacements on mass movements from repeat optical images. In the first approach, image intensities are interpolated to a desired sub-pixel resolution using a bi-cubic interpolation scheme prior to the actual displacement matching. In the second approach, the image pairs are correlated at the original image resolution and the peaks of the correlation coefficient surface are then located at the desired sub-pixel resolution using three techniques, namely bi-cubic interpolation, parabola fitting and Gaussian fitting. Both principal approaches are applied to three typical mass movement types: rockglacier creep, glacier flow and land sliding. In addition, the influence of pixel resolution on the accuracies of displacement measurement using image matching is evaluated using repeat images resampled to different spatial resolutions. Our results show that bi-cubic interpolation of image intensity performs best followed by bi-cubic interpolation of the correlation surface. Both Gaussian and parabolic peak locating turn out less accurate. By increasing the spatial resolution (i.e. reducing the ground pixel size) of the matched images by 2 to 16 times using intensity interpolation, 40% to 80% reduction in mean error in reference to the same resolution original image could be achieved. The study also quantifies how the mean error, the random error, the proportion of mismatches and the proportion of undetected movements increase with increasing pixel size (i.e. decreasing spatial resolution) for all of the three mass movement examples investigated.

1. Introduction

Present climatic change shifts geomorphodynamic equilibriums and intensifies related mass movement processes such as landslides and permafrost creep (Haeberli & Beniston, 1998; Rebetez et al., 1997). Extension and intensification of human activities in areas affected by such mass movements increase the probability of connected adverse impacts like natural hazards or building stability problems. A growing number of remote sensing opportunities exist to monitor such mass movements. The increasing number of available collections of multi-temporal space-borne, air-borne and terrestrial images, and the improvements in remote sensing and image processing in general significantly enhance the potential for applying matching techniques to detect and quantify Earth surface mass movements from repeat remotely sensed data. These needs and developments call for continued efforts to improve terrain displacement matching methods based on repeat images for a large number of applications in Earth sciences.

Image matching is a group of techniques of finding corresponding features or image patches in two or more images taken of the same scene from different viewing positions, at different times and/or using different sensors. Image matching is used for a large variety of applications such as image (co-)registration, stereo parallax matching for generation of digital elevation models, particle image velocimetry (PIV), or displacement measurements (Brown, 1992; Westerweel, 1993; Zitová & Flusser, 2003).

The group of area-based matching techniques is the most widely used method due to its relative simplicity (Zitová & Flusser, 2003). Cross-correlation, particularly in its normalised form which accounts for brightness and contrast in image sequences, is the most widely used similarity measure of this method due to its reliability and simplicity (Lewis, 1995). The normalised cross-correlation (NCC) algorithm has been used to investigate Earth mass movements such as glacier flow, rockglacier (used here as one word after Barsch (1996)) creep and land sliding in many empirical studies (e.g. Haug et al., 2010; Kaufmann & Ladstädter, 2003; Kääb, 2005; Kääb & Vollmer, 2000; Quincey et al., 2005; Scambos et al., 1992; Scherler et al., 2008; Skvarca et al., 2003; Taylor et al., 2008; Wangensteen et al., 2006).

Although NCC has been documented to be simple and reliable, a number of drawbacks have been reported as well (Lewis, 1995; Scambos et al., 1992; Zhao et al., 2006). Firstly, NCC is sensitive to noise in the images. Secondly, NCC is sensitive to significant scale,

* Corresponding author. Tel.: +47 22857869; fax: +47 22854215.
E-mail addresses: m.d.gilo@geo.uio.no (M. Debella-Gilo), kaeaeb@geo.uio.no (A. Kääb).

0034-4257/$ – see front matter © 2010 Elsevier Inc. All rights reserved.
doi:10.1016/j.rse.2010.08.012

rotation or shearing differences between the images to be correlated. Thirdly, for the measurement to be reliable the displacement has to be greater than the mean error of the image (co-)registration. Fourthly, the precision of NCC is, in principle, limited to one pixel, and thus varies with the pixel size of the image data used.

Pixel-level accuracy might be satisfactory depending on the spatial resolution of the imagery available and the type of process being investigated. Improving NCC precision, however, improves displacement accuracy two fold: by reducing the image co-registration error and by improving the matching accuracy directly. To achieve sub-pixel precision in NCC, two approaches can be used. The first option is to resample the image intensity to a higher spatial resolution through interpolation. This approach has been applied in stereo matching (e.g. Szeliski & Scharstein, 2002) and in displacement measurement of Earth surface movements (e.g. Crippen & Blom, 1991; Yamaguchi et al., 2003). The second option is to interpolate the cross-correlation surface after the matching process to a higher spatial resolution in order to locate the correlation peak with sub-pixel precision. This approach has been applied in image registration (e.g. Althof et al., 1997; Scambos et al., 1992), in mechanics to measure the velocity of particles (e.g. Westerweel, 1993; Willert & Gharib, 1991), in motion tracking to measure displacements of landslide (e.g. Delacourt et al., 2004; Yamaguchi et al., 2003) and glaciers (e.g. Scambos et al., 1992). There are also area-based spatial domain methods that are intrinsically capable of sub-pixel precision such as the least squares matching, which is more often used in stereoscopic DEM generation and image registration. Least square matching is known for its capability to deal with scaling and rotation and has occasionally been used in the displacement measurement of mass movements (e.g. Kaufmann & Ladstädter, 2003; Whillans & Tseng, 1995). Other techniques that are used in mass movement analysis for achieving sub-pixel precision are the Fourier-based phase matching and gradient-based matching (e.g. Haug et al., 2010; Leprince et al., 2007; Taylor et al., 2008). Pre-processing steps such as noise filtering and post-processing steps such as filtering of displacement vectors by averaging are also able to improve the precision and accuracies of displacement estimates (Kääb & Vollmer, 2000; Zitová & Flusser, 2003).

The present study focuses exclusively on mass movement analysis by NCC due to the wide-spread use of this technique, and its simplicity and reliability. Thus, we do not consider the above methods that are intrinsically capable of sub-pixel precision. Further, we concentrate on the intensity interpolation and the correlation interpolation approaches because both are generic and independent of image resolution. There is no study available that rigorously compares the relative performance of the two approaches when measuring the displacement of mass movements from repeat images.

Mass movement, in the context of our study, refers to the down-slope movement of Earth materials including rocks, glacier ice and debris triggered by agents such as gravity, water, and tectonic activity (Ritter, 2006). Many Earth surface mass movements such as landslide, glacier flow, and rockglacier creep are characterized by displacement rates of the same order of magnitude as the spatial resolution of the space-borne or air-borne imagery typically available for their measurement. Such masses usually move with rates in the order of several centimetres to some hundred meters per year. Sub-pixel precision of image matching algorithms, here NCC, therefore has a large potential to improve the signal-to-noise ratio of the measurements. In other words, improving the precision (i.e. level of detail of the measurement) of displacement estimation contributes to the improvement of accuracy (i.e. the certainty of the estimation).

Using NCC as an example, this study compares the accuracies of two fundamentally different approaches to reaching sub-pixel precision in mass movement measurement from repeat remotely sensed images, namely intensity interpolation and correlation interpolation. The study specifically aims at (i) quantifying the effects of pixel size (i.e. ground area represented by a pixel) on the accuracy of displacement matching, (ii) quantifying and comparing the performances of different sub-pixel precision algorithms, and (iii) identifying the gains and limit of the sub-pixel precision algorithms.

2. Methods

2.1. Image data and resolution pyramid

For this study, three different types of mass movements were selected based on their frequency in high mountain areas: land sliding, glacier flow, and rockglacier creep. Three temporal pairs of airphotos each covering ground areas of 0.35 km^2, 3 km^2 and 0.25 km^2 respectively were used. These images were orthorectified prior to displacement matching. Details are given in Section 3.

Better understanding of the influence of spatial resolution on the accuracy of image matching requires images of the same area taken at the same time, under the same flight and ground conditions, but using sensors with different spatial resolutions. Such conditions are not easily met. Instead, different optical systems were simulated by down-sampling the original high-resolution aerial orthoimages to five levels of lower spatial resolution (Table 1). One resolution pyramid with six levels each was finally obtained for each of the two repeat images of each of the three mass movements as shown in Fig. 1. The resolution pyramids are thus not the same as the Gaussian or Laplacian image pyramids often used in multi-scale image analysis or in image visualisation. The down-sampling factors here are chosen for convenience. The down-sampling was performed using the MATLAB module '*imresize*' with the most efficient and reliable algorithm for this purpose, namely bi-cubic convolution. The algorithm assigns the weighted average of pixel values in the nearest 4-by-4 neighbourhood (Keys, 1981). Although this resampling process is slightly different from the pure signal averaging happening in the instantaneous field of view of a sensor detector cell, we decided to choose bi-cubic convolution because most images used for matching will in practice have undergone such interpolation during image correction and pre-processing steps, such as orthorectification (Toutin, 2004).

Additionally, one resolution pyramid was created from one of the original glacier images after applying a two-dimensional translation of 15 pixels (9 pixels in the x-direction and 12 pixels in the y-direction). This translation becomes a non-integer pixel displacement in the lower resolution resampled images. Since this pair was made from just one original image and the displacement applied was only translation, the pair serves as a control data set as it is free of noise from temporal surface changes, changes in imaging condition, registration errors and geometric distortions.

Table 1
Movement process types, spatial resolution of the original images and resolution pyramids used in this study, and examples of satellite sensors simulated by this image resolution resampling.

Mass movement type	Resampling factor	Ground pixel size (m)	Examples of optical satellite systems simulated
Rockglacier and landslide	Original	0.2	
	2	0.4	IKONOS, WorldView-1
	4	0.8	IKONOS, QuickBird
	8	1.6	QuickBird
	16	3.2	SPOT 5 panchromatic, ALOS(PRISM)
	32	6.4	SPOT 5 panchromatic
Glacier	Original	0.5	
	2	1	IKONOS
	4	2	IKONOS, QuickBird, SPOT 5 panchromatic, ALOS (PRISM)
	8	4	SPOT 5 panchromatic
	16	8	SPOT panchromatic
	32	16	ASTER, Landsat 7 panchromatic

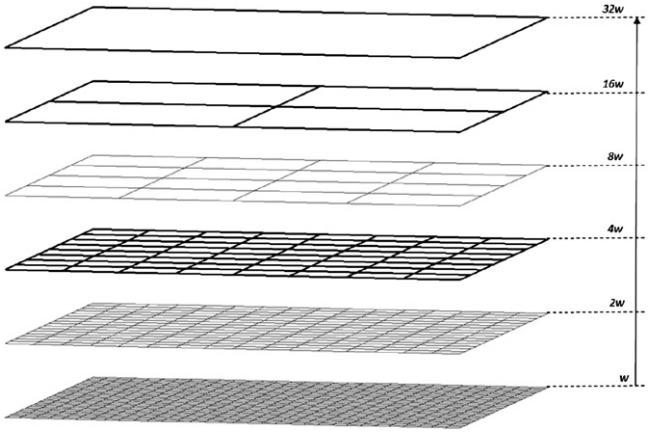

Fig. 1. Setup of the image resolution pyramid, w being the ground pixel size (GPS) of the original image.

2.2. Normalised cross-correlation

The normalised cross-correlation (NCC) algorithm is a similarity measure that is used in image matching to measure the similarity between matching entities in one image and their corresponding entities in the other image. The algorithm was developed based on the concept of distance measure but second normalised to account for the differences in brightness and contrast (Lewis, 1995; Vosselman et al., 2004). An image I_1 over an area is taken at time T_1 and another image I_2 over the same area at time T_2 (Fig. 2). The term f(x, y) stands for the intensity values of a squared area that is a subset of I_1, t(x−u, y−v) for the intensity values in a squared area in I_2 of the same size as f(x, y), where u and v are integer pixel offsets in x- and y-direction respectively. f(x, y) is further called reference template and t(x−u, y−v) is called search template. The size of the template is chosen to be large enough to maximize the signal-to-noise ratio and small enough to minimize velocity gradients (Kanade & Okutomi, 1991). The search area size is chosen to be large enough to include the farthest moving template and small enough to limit the computational cost of the matching. To find the corresponding square to f(x, y) in I_2, the normalised cross-correlation coefficient (ρ) between f(x, y) and corresponding window in I_2, t(x−u, y−v), is computed. The NCC coefficient ρ is computed as given in Eq. (1) and is assigned to the central pixel of the template (Lewis, 1995; Vosselman et al., 2004). The computation continues by moving t in every iteration by 1 pixel until the entire search window is covered. After finishing the computation, the pixel (x_0, y_0) in the search window with the highest correlation coefficient is considered as the likely best match for the central pixel of the reference template. The Euclidean distance between the coordinates of the reference point [x, y] and the matching point $[x_0, y_0]$ is considered as the horizontal displacement magnitude, d(x, y).

$$\rho(\mathbf{x},\mathbf{y}) = \frac{\sum_{\mathbf{x},\mathbf{y}}\left(f(x,y)-\bar{f}\right)\left(t(x-u,y-v)-\bar{t}\right)}{\left(\sum_{\mathbf{x},\mathbf{y}}\left(f(x,y)-\bar{f}\right)^2\sum_{\mathbf{x},\mathbf{y}}\left(t(x-u,y-v)-\bar{t}\right)^2\right)^{1/2}}. \quad (1)$$

$\bar{f}$ is the mean of the intensities in the reference template f(x, y) and $\bar{t}$ is the mean of the intensities in the search template t(x−u, y−v). The values of ρ range between −1 (when the matching entities are inverses of each other) and 1 (when the matching entities are exactly the same). ρ = 0 is an indication of no relationship between the matching entities. Even if there is no truly corresponding entity in the search image, there will always be some peak correlation coefficient. Therefore, it is necessary to decide a threshold for ρ below which the match is rejected.

2.3. Matching and displacement measurement at different pixel sizes

First, the original high-resolution orthoimages (before resampling) were matched using the NCC algorithm at pixel-precision to determine the matching positions and compute the horizontal displacement magnitude and direction. Mismatches that were characterized by low peak correlation coefficients, very large displacements in relation to their neighbouring templates, or displacements showing distinct upslope movement were removed manually. Since manual removal of the mismatches is heuristic and influences the final analysis, the proportion of mismatches is counted and reported separately as an indicator of performance. Additionally, displacements less than the mean orthorectification error were removed as they are not reliably distinct from the error. The orthorectification error (offset between the images) was computed by matching stable grounds. The computation revealed that a maximum of 1 pixel offset exists in each dimension at the resolution of the original orthoimages. In orthoimages, positional errors increase radially from the projection centre proportional to the magnitude of the vertical errors in the digital elevation model used for the orthoprojection. All our three mass movements are located near the centres of the original air photos and the stable grounds are located towards the edges. Therefore, the here-estimated offset error is assumed to exceed the actual positional errors on the mass movements. The matching results on the original full-resolution images

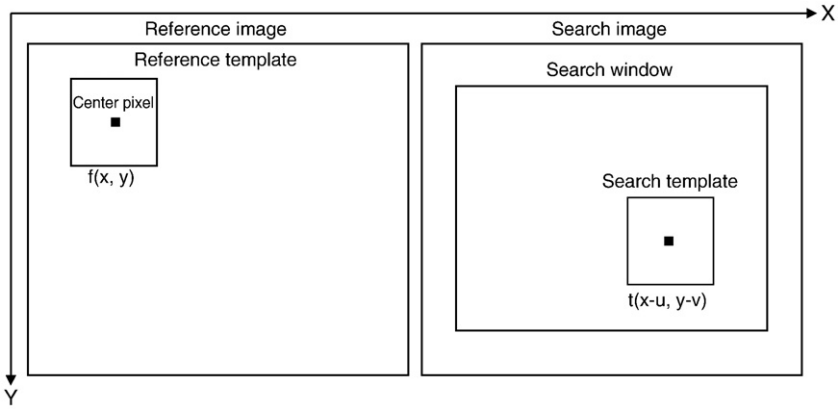

Fig. 2. Scheme of the image pairs together with the reference template, central pixel, search template and the search window.

were considered as reference for all other measurements throughout the resolution pyramid pairs.

Matching and displacement measurement were in a next step performed on all resolution levels of the resolution pyramid pairs for all locations used also above for the original images. The absolute sizes and positions of the reference templates and the search windows were kept constant in ground coordinates throughout the resolution pyramid by adjusting the number of pixels according to the resolution. This procedure was in order to avoid variations in signal content as a result of inclusion or exclusion of ground features. In other words, the ground area covered by the templates remained the same when the respective image resolution changed. The size of the template was kept at around 26 m and 65 m for the originally 0.2 m and 0.5 m resolution images, respectively. The size of the search window was kept at around 102 m and 265 m for the originally 0.2 m and 0.5 m resolution images, respectively, so that it certainly included the expected maximum surface displacement.

The performance of the matching at different resolutions was evaluated by comparing the obtained matching position to those obtained from the image pairs at original full resolutions. Often, the accuracy of displacement measurements using cross-correlation is evaluated by comparing the estimated displacement magnitude (d_i) to the actual displacement magnitude (d_0). In this study, this is found to be misleading as the displacement direction is equally important to assess the matching accuracy. Therefore, instead of using the difference in displacement magnitude as an indicator of accuracy, we use the shift in matching position (Fig. 3). The matching positions obtained during the correlation of the original images [x_0, x_0] are considered as references. All the matching positions at the different coarser or back-interpolated (see next section) resolutions [x_i, y_i] are compared to these reference positions. The magnitude of this deviation (*dev*) is here used as measure for the performance of the image and algorithm used (Eq. 2).

$$dev = \sqrt[2]{(\mathbf{x_i}-\mathbf{x_0})^2 + (\mathbf{y_i}-\mathbf{y_0})^2}. \quad (2)$$

The image and algorithm performance was evaluated based on three types of errors known in image matching, namely mismatches (spurious matches), mean bias (here mean deviation) and the root mean square (RMS) error (Huang et al., 1997; Lourenco & Krothapalli, 1995). Additionally, the proportion of undetected movements was also added as a measure of the influence of pixel size on the success of displacement measurements. The mismatches and the undetected moving entities were counted globally while the magnitudes of the mean deviation and the RMS were computed locally (Eqs. 3 and 4). Here, n stands for the total number of validly matched entities and i stands for the individual validly matched entity.

The mean deviation $\left(\overline{dev}\right)$ is given as:

$$\overline{dev} = \frac{\sum_{\mathbf{i}=1}^{\mathbf{n}} dev_{\mathbf{i}}}{\mathbf{n}}. \quad (3)$$

And the RMS (σ_{dev}) is given as:

$$\sigma_{dev} = \sqrt[2]{\frac{\sum_{i=1}^{n}\left(dev_i-\overline{dev}\right)^2}{n-1}}. \quad (4)$$

2.4. The sub-pixel precision approaches

2.4.1. Intensity interpolation

The issue of sub-pixel estimation appears because the images available are often not at the optimal resolution for precise quantification of movement. Signals in image pixels are created by integrating spatially continuous signals over the area covered by the pixel. If the continuous signal existed, one could choose the interval at which the integration is done, i.e. the pixel resolution, as long as the signals are detectable. However, since such integration of continuous signals is done by the imaging sensor during the image acquisition, the continuous signal is no longer available for later analysis. One alternative is thus to reconstruct the continuous signal from the spatially discrete images. Full reconstruction is only ideally possible, though. Therefore, the image itself is interpolated to the desired pixel resolution using certain interpolation schemes, preferably ones that can effectively reduce aliasing.

In this study, the coarse resolution images within the above-computed resolution pyramids were back-interpolated to different finer resolutions using the MATLAB-based '*imresize*' module with the bi-cubic interpolation scheme (Fig. 4 left). The bi-cubic algorithm is an appropriate choice for accuracy and efficiency in comparison with other algorithms (Keys, 1981; Meijering & Unser, 2003). After such back-interpolation, the NCC algorithm with Eq. (1) was applied using the same templates and search windows as used in the original reference image pairs. The interpolation is done on the fly for each reference template and search window, and not for the entire image before the matching process to cope with MATLAB's memory restrictions. Even in this approach when the resampling factor is doubled, the computation time increases about four times.

2.4.2. Similarity interpolation

The similarity measure used in this study, i.e. the NCC coefficient, produces pixel-level peak locations. However, that location might not be the exact position of the matching entity. To find the sub-pixel position from the discrete NCC coefficients, one can either interpolate

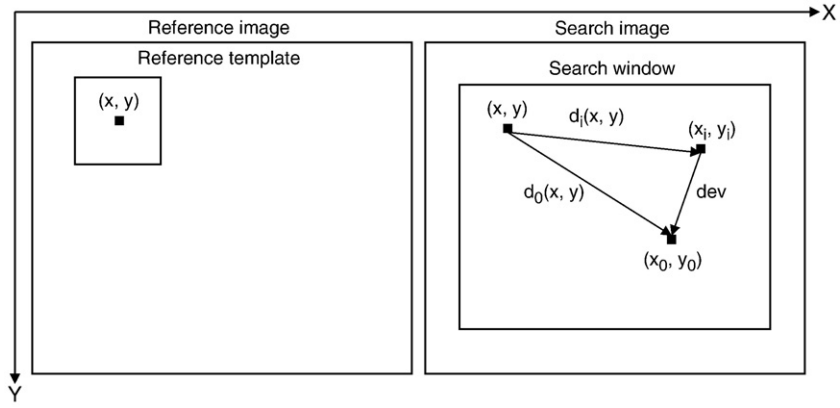

Fig. 3. Scheme of the matching position deviations and the difference in displacement.

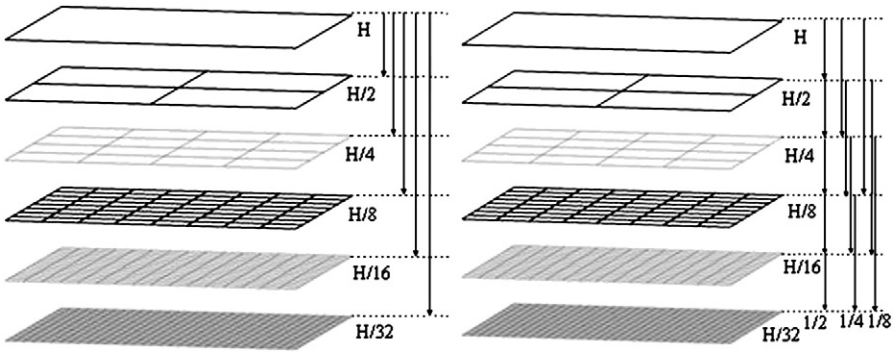

Fig. 4. Schematic setup of intensity and correlation interpolation of the coarsest resolution images to different sub-pixel details (left) with the different possible alternatives of assessing sub-pixel performance (right). H stands for GPS of the coarsest resolution images.

the cross-correlation surface to a higher resolution using two-dimensional interpolation algorithms or fit a two-dimensional analytical function to the correlation surface around the peak.

2.4.2.1. Correlation interpolation using bi-cubic convolution. The correlation surface around the peak is resampled to the desired higher resolution. A two-dimensional cubic convolution of the correlation coefficients is then applied to the resampled grid using the MATLAB module '*interp2*'. The bi-cubic convolution takes the weighted average of the nearest 16 (4-by-4) pixels. The peak is then relocated at the new resolution.

2.4.2.2. Curve fitting. As an alternative to peak interpolation, one can also create a continuous function that optimally fits the correlation coefficient data and compute the precise location of the peak from the maximum of the function. The challenge is that no single function can usually perfectly describe the cross-correlation surface. However, the fact that the correlation surface around its peak often approaches a bell shape can be exploited. Therefore, two-dimensional polynomial functions can approximate the surface. A number of models have been tested in empirical and theoretical researches, particularly in particle image velocimetry (PIV), though with varying successes (Nobach & Honkanen, 2005; Westerweel, 1993; Willert & Gharib, 1991). Parabola and Gaussian fitting are tested here for mass movement analysis, as these have shown successes in other areas, especially in PIV.

In parabola fitting, the shape of the correlation surface is assumed to fit two orthogonal parabolic curves. The location of the 'actual' peak is computed by independently fitting one dimensional quadratic function and computing the location of the peak (Nobach & Honkanen, 2005; Shimizu & Okutomi, 2002; Westerweel, 1993). Let's assume that we have computed the pixel level (integer) position of the peak as $[x_0, y_0]$. This pixel has two neighbours in each of the two orthogonal directions: (x_0-1) and (x_0+1) in the x-direction and (y_0-1) and (y_0+1) in the y-direction. To find the sub-pixel peak position in each direction $(x_0+\Delta x, y_0+\Delta y)$, we define a parabolic curve that connects the three points of that direction and compute the position where the curve attains its maximum. Eqs. (5) and (6) compute the non-integer location of the peak in the x- and y-directions which will then be added to the pixel (integer).

$$\Delta X = \frac{\rho(X_0-1,Y_0)-\rho(X_0+1,Y_0)}{2\rho(X_0-1,Y_0)-4\rho(X_0,Y_0)+2\rho(X_0+1,Y_0)} \quad (5)$$

$$\Delta Y = \frac{\rho(X_0,Y_0-1)-\rho(X_0,Y_0+1)}{2\rho(X_0,Y_0-1)-4\rho(X_0,Y_0)+2\rho(X_0,Y_0+1)}. \quad (6)$$

Likewise, in Gaussian fitting, the bell shape of the correlation surface is assumed to fit a 2D Gaussian function (Nobach & Honkanen, 2005; Westerweel, 1993; Willert & Gharib, 1991). It is assumed that the two dimensions are separable and orthogonal. Thus, the sub-pixel peak location is calculated separately for the two directions by fitting a second-order polynomial to the logarithm of the maximum sample and the direct neighbours as in Eqs. (7) and (8).

$$\Delta X = \frac{\ln(\rho(X_0-1,Y_0))-\ln(\rho(X_0+1,Y_0))}{2\ln(\rho(X_0+1,Y_0))-4\ln(\rho(X_0,Y_0))+2\ln(\rho(X_0-1,Y_0))} \quad (7)$$

$$\Delta Y = \frac{\ln(\rho(X_0,Y_0-1))-\ln(\rho(X_0,Y_0+1))}{2\ln(\rho(X_0,Y_0+1))-4\ln(\rho(X_0,Y_0))+2\ln(\rho(X_0,Y_0-1))} \quad (8)$$

2.5. Evaluation of different levels of sub-pixel detail

Section 2.4 evaluates which sub-pixel approach performs best in improving the precision and accuracy of NCC-based image matching. It is also important to know how far sub-pixel interpolation of coarse resolution image intensities or the correlation surface is able to substitute pixel-level matching of images of the corresponding but original resolution, as well as the sub-pixel detail at which the interpolation to achieve sub-pixel precision can no longer sufficiently substitute image of that resolution. The sub-pixel precision matching is thus computed at different levels of the resolution pyramid and its performance is evaluated in reference to the pixel-level matching of images with the same but original resolution. This procedure becomes clearer with an example: suppose we want to know the performance of sub-pixel precision matching at the level of half a pixel. This can be achieved by taking an image of, for instance, 8 m resolution, computing the sub-pixel precision matching to 4 m and comparing the latter sub-pixel performance to the performance of pixel-level matching of an image with 4 m original resolution. Alternatively, one can take a 4 m resolution image, compute its sub-pixel resolution matching to 2 m and compare the performance of the latter in relation to a 2 m resolution original image. In our study, this procedure is iterated for the entire pre-processed resolution pyramid and all resolution steps included in it, not just the level-factor 2 exemplified here (Fig. 4 right).

Eq. (3) was used to evaluate the deviation between the sub-pixel matching and the pixel-level matching at corresponding image resolutions. This time, the reference matching position $[x_0, y_0]$ is the matching position obtained for the same template by using a pixel-level matching of an image pair of a resolution equal to the resolution to which the sub-pixel algorithm is conducted. If the sub-pixel matching between two coarse images exactly substitutes pixel-level matching of images with corresponding fine resolution, there will be no deviation between the two matching positions.

In addition to the performance evaluation parameter *dev* as explained above, the proportion by which each error term of the pixel-level precision was reduced by a sub-pixel algorithm was used as an alternative indicator for the accuracy improvement. For

example, if an algorithm i was used, its performance in reducing the mean deviation from the pixel-level algorithm mean deviation is given as in Eq. (9).

$$per_i = \frac{\left(\overline{dev_i} - \overline{dev_P}\right) * 100}{\overline{dev_P}} \quad (9)$$

Here, per_i is the percentage reduced mean bias when sub-pixel algorithm i is used, $\overline{dev_i}$ is the mean bias of that algorithm, and $\overline{dev_p}$ is the mean deviation of the pixel-level NCC algorithm.

3. Test sites

As an example for glacier flow, we use the glacier Ghiacciaio del Belvedere. It is located below the Monte Rosa peak, above Macugnaga and the Anzasca valley of the Italian Alps (approx. 7°54′39″ E, 45°54′39″ N). This glacier has recently become known for its surge-type movement (Haeberli et al., 2000; Kääb et al., 2004). It is a very dynamic glacier with a history of flooding and hazardous incidences. Since the glacier was at the time of photography very dynamic with high surface speeds, the images chosen for the present study were taken on 6 September and 11 October 2001 with a temporal baseline of around one month and an orthoimage pixel resolution of 0.5 m. More details on the images and the glacier can be found in Kääb et al. (2005).

Rockglaciers consist of permanently frozen debris that slowly deforms down-slope under gravity. The rockglacier chosen as test site for this study is located in the Muragl valley of the Upper Engadine area of the Swiss Alps (approx. 9°55′30″ E, 46°30′15″ N). It has been under investigation for decades using technologies such as photogrammetry, geodesy and geophysics to understand the mechanics of the rockglacier (Kääb, 2002; Kääb & Vollmer, 2000). The previous studies showed maximum creep speeds of up to 0.5 ma^{-1}. The orthoimages used in the present study were based on aerial images taken on 7 September 1981 and 23 August 1994 with 13 years of temporal baseline and 0.2 m of spatial resolution.

The Aletsch rockslide, used here as an example for a slow landslide, is located near the tongue of the Aletsch Glacier, Canton of Valais, Swiss Alps (approx. 8°01′28″ E, 46°24′11″ N). The driving force behind the rockslide is the continuous retreat of the Aletsch Glacier since approximately 1850 causing debuttressing of the adjacent slopes (Kääb, 2002; Kääb et al., 2005). A study that investigated the velocity of the rockslide between 1976 and 1995 showed that the rock masses have moved up to 2 m on average over 19 years (Kääb, 2002). The orthoimage pair used in the present study is based on air photos taken on 6 September 1976 and 5 September 2006 with 30 years temporal baseline and 0.2 m spatial resolution.

4. Results

4.1. Displacement vectors of the three different mass movements

Table 2 summarises displacement statistics for the three mass movements investigated. The results were produced from the analyses of the original orthoimages after filtering all the mismatches. One can see that the glacier moves fast as compared to the rockglacier and the even slower moving rockslide. Figs. 5–7 present the displacement vectors of the three mass movements systematically sampled at 128 pixels in both dimensions. Image matching showed that also the stable ground in the scene show non-zero displacements due to the presence of systematic image (co-)registration errors. However, after filtering of the vectors based on the estimated overall image registration error of one pixel, after thresholdinig of the correlation coefficients (0.65 for the rockglacier, 0.6 for the glacier and 0.45 for the landslide) and after excluding upslope movements, only the remaining vectors presented in the figures are considered to be valid and useful as reference.

4.2. Pixel resolution and matching accuracy

As expected, Fig. 8 (A) shows for all the three mass movement types that, as the pixel size increases, the mean deviation $\left(dev\right)$ also increases. There is no observable difference among the three mass movements on this type of error. The control matching shows that the mean deviation increases linearly with the factor by which the pixel size increases. In fact, the mean deviation is about half a pixel at every resolution, and similar for the real mass movement images. However, at larger pixel sizes the deviations for the real mass movements tend to be lower than a linear increase between pixel size and mean deviation, as opposed to that of the control image set which maintains the linear relationship.

The random error (RMS) shows a similar pattern except that it is very low at small pixel sizes (Fig. 8 B). The trend in RMS for the landslide appears to be higher than for the other two sites, with that for the glacier being the lowest. The control does not have any random error until the pixel size is increased by the factor of 8.

The proportion of mismatches (Fig. 8C) dramatically increases with increasing pixel size. There appear to be fewer mismatches for the glacier compared to the other mass movement types for the same metric pixel resolution. In the case of the control set, there was no mismatch observed until the pixel size was increased by the factor of 8.

The proportion of undetected moving templates also increases with pixel size (Fig. 8D). There seems to be no difference between the rockglacier and the landslide, but for the glacier the proportion is lower at comparable resolutions. Movements are undetected when the pixel size is greater than the displacement. That can practically be observed in the case of the control which has a uniform translation of 7.5 m over the whole image. All of the movements were detected as long as the pixel resolution was kept less than 8 m. However, as soon as the pixel resolution became 16 m, about 50% of the moving entities were not detected. In the case of the three mass movements, undetected movements were first observed after the pixel size was doubled. This is due to the existence of slow movements in all scenes that could be missed in resolution pyramid levels with comparably fine resolution. At a pixel resolution of 6.4 m approximately 35% of the original landslide and rockglacier movements and 65% of the original glacier movements could be detected.

Table 2
Summary statistics for the displacement magnitudes and average horizontal speed of the mass movements and the translation-only control image as estimated from the matching of the original full-resolution orthoimages.

Mass movement	Temporal baseline	Mean displacement (m)	Maximum displacement (m)	Standard deviation of displacement (m)	Maximum speed (ma^{-1})
Aletsch rockslide	30 years	1.5	4.2	0.45	0.14
Muragl rock glacier	13 years	2.4	5.8	1.20	0.45
Ghiacciaio del Belvedere glacier	1 month	12.22	18.83	5.0	226
Control (translation-only)		7.50	7.50	0	7.50

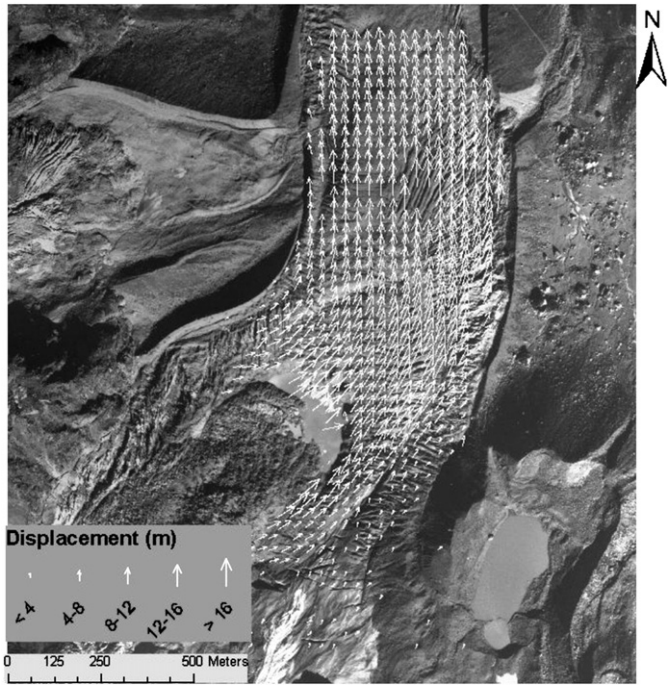

Fig. 5. Displacement vectors on the Ghiacciaio del Belvedere (Sept.– Oct. 2001) as estimated by matching the original orthoimages and systematically sampled at 128 pixels interval in each dimension. The image displayed is from Oct. 2001.

4.3. Accuracies of the sub-pixel precision algorithms

In this section we present the results of the test described in Section 2.4. Figs. 9 and 10 depict the mean deviation *dev* of the matching positions against the sub-pixel precisions of each of the algorithms for the control set and the three mass movements respectively. The magnitudes of Fig. 10 are created by averaging the values obtained for the three mass movement types as the trend is similar for all the three. Both figures show that interpolation of the image intensity before matching results in the best matching accuracy. In the control set, the bi-cubic interpolation of intensity and correlation perform alike up to the precision of 0.25 pixel below which they clearly separate. The bi-cubic interpolation of the correlation surface follows the intensity interpolation. The curve fitting using the parabola and Gaussian models performs better than bi-cubic interpolations to only one half of the original pixel size. For the real mass movements, there is very little accuracy gain by interpolating to lower than 0.1 pixels. The control result shows that when the movement is only translation, the magnitude of the deviation is very low. Besides, it seems that for the control set interpolation to more detail level than 0.1 pixels improves the accuracy even further.

4.4. Relative performance of the algorithms at different sub-pixel details

This section presents how much each level of sub-pixel detail substitutes original images of the same resolution. The setup of this test is described in Section 2.5. Fig. 11 shows the mean deviation between the matching position of the interpolated image pairs and the matching of the reference image pairs, against the factor of resolution difference between the original reference and the coarse image. Results are presented for the control set and the three mass movement types.

Fig. 11(A) shows that when the difference between the images is only the here-applied translation, sub-pixel interpolation of the image intensities up to 1/8th of the original pixel size prior to matching can perfectly substitute images of comparable original resolution. This exact substitution can be achieved by using bi-cubic interpolation of the correlation surface only up to 1/4th of the original pixel size. For example, a 16 m resolution image interpolated to 2 m using bi-cubic interpolation before matching performs exactly as a 2 m resolution image pair as long as there is no other source of difference between the image pairs than rigid translation. But when the level of detail goes beyond 1/8th, there appears to be a deviation between the two. The magnitude of these numbers depends, of course, on the translation magnitude applied in the control set. However, the test shows the better performance of bi-cubic intensity interpolation over the other sub-pixel algorithms tested.

For all the real mass movement types, as the difference in pixel size between the coarse resolution and the reference resolution increases, the deviation (dev) of the sub-pixel matching position from the matching position of the same, but original image resolution, increases regardless of the algorithm (Fig. 11B, C and D). This means, not

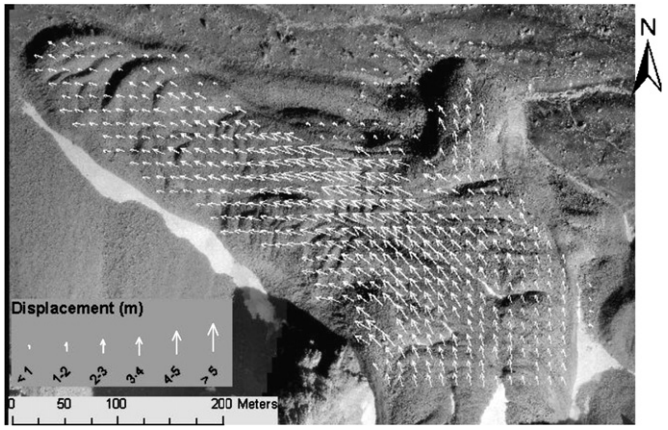

Fig. 6. Displacement vectors on the Muragl rockglacier (1981–1994) as estimated by matching the original orthoimages and systematically sampled at 128 pixels interval in each dimension. The image displayed is from 1992.

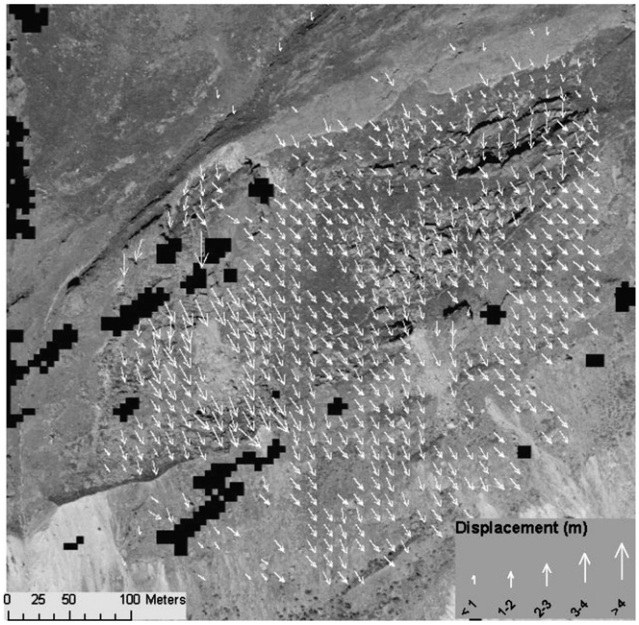

Fig. 7. Displacement vectors on the Aletsch rockslides (1976–2006) as estimated by matching the original orthoimages and systematically sampled at 128 pixels interval in each dimension. The image displayed is from 2006. Aletsch Glacier is to the lower right.

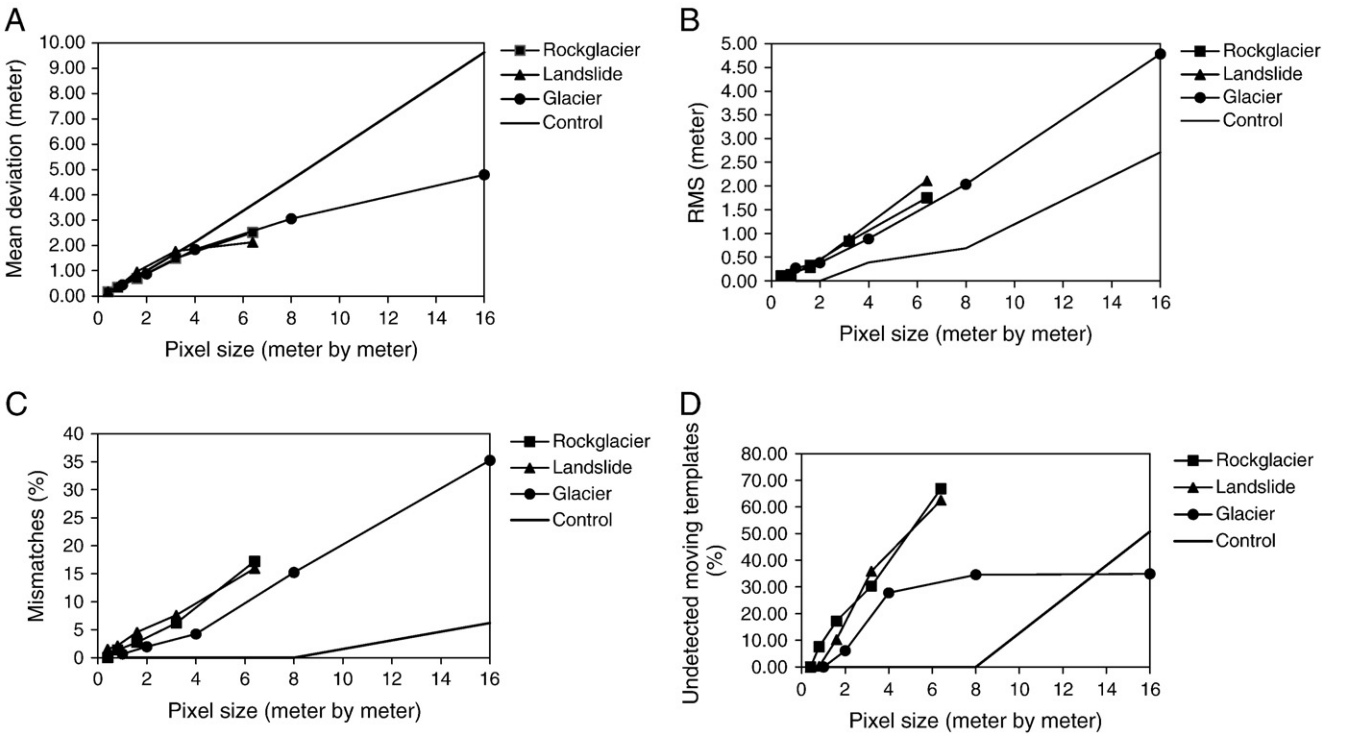

Fig. 8. Mean deviation (A), RMS (B), percentage mismatches (C) and percentage undetected moving templates (D) for the three mass movement types and the translation-only control set for varying pixel resolutions.

surprisingly, that the sub-pixel algorithm resembles images of comparable resolution less and less as the sub-pixel detail increases. At every resolution, the mean deviation is the lowest when intensity interpolation was used before matching followed by the bi-cubic interpolation of the correlation surface. The parabola- and Gaussian-based peak localisations perform poorer and alike. This confirms the above results based on the control set.

Remarkably, at a certain level of sub-pixel detail, the deviation between the sub-pixel algorithm and same resolution original image becomes high enough that further interpolation has no meaningful advantage. For the real mass movements used in this study, such level of detail is about 1/16th although the control set gives less deviation even at greater level of detail.

Similar performance is observed for the RMS although the differences are not as clear as for the mean deviation. Noticeably, the RMS of the pixel-precision matching of the control set is lower than that of the similarity interpolation whichever algorithm is chosen. For the real mass movements the lowest RMS is recorded for intensity interpolation followed by similarity interpolation using the bi-cubic, parabolic and Gaussian algorithms.

No clear difference is observed among the algorithms in the proportion of mismatches. One of the advantages of sub-pixel algorithms is locating the exact position within the pixel and thus the detection of all movements as long as the resolution at which the interpolation is conducted is less than the displacement. This implies that when using low-resolution images, slow moving terminus and margins of the masses are hardly detected. For example, Fig. 13 shows non-zero displacement vectors computed by matching images of 3.2 m GPS without sub-pixel interpolation (black vectors) and after sub-pixel interpolation of the images to 0.4 m GPS using bi-cubic interpolation (white vectors). As can be seen from the regions indicated by the four thick black arrows, slow motions, as typically found for e.g. towards the margins and terminus of a rockglacier, are detected only using sub-pixel interpolation. Success of displacement measurement from repeat images therefore varies spatially depending on the GPS of the images and the displacement magnitude of the moving masses.

The decrease in errors due to the sub-pixel algorithms was also quantified as a measure of accuracy gain (per_i) or as a measure of how

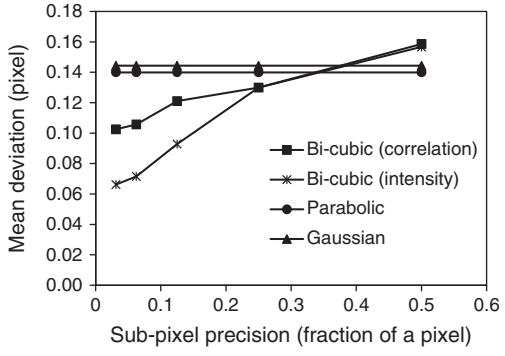

Fig. 9. Comparison of the different sub-pixel precision approaches for the translation-only control image set.

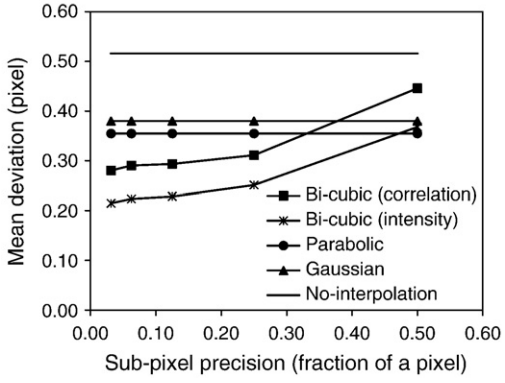

Fig. 10. Comparison of the different sub-pixel precision approaches for the real mass movements averaged from the three mass movement types investigated.

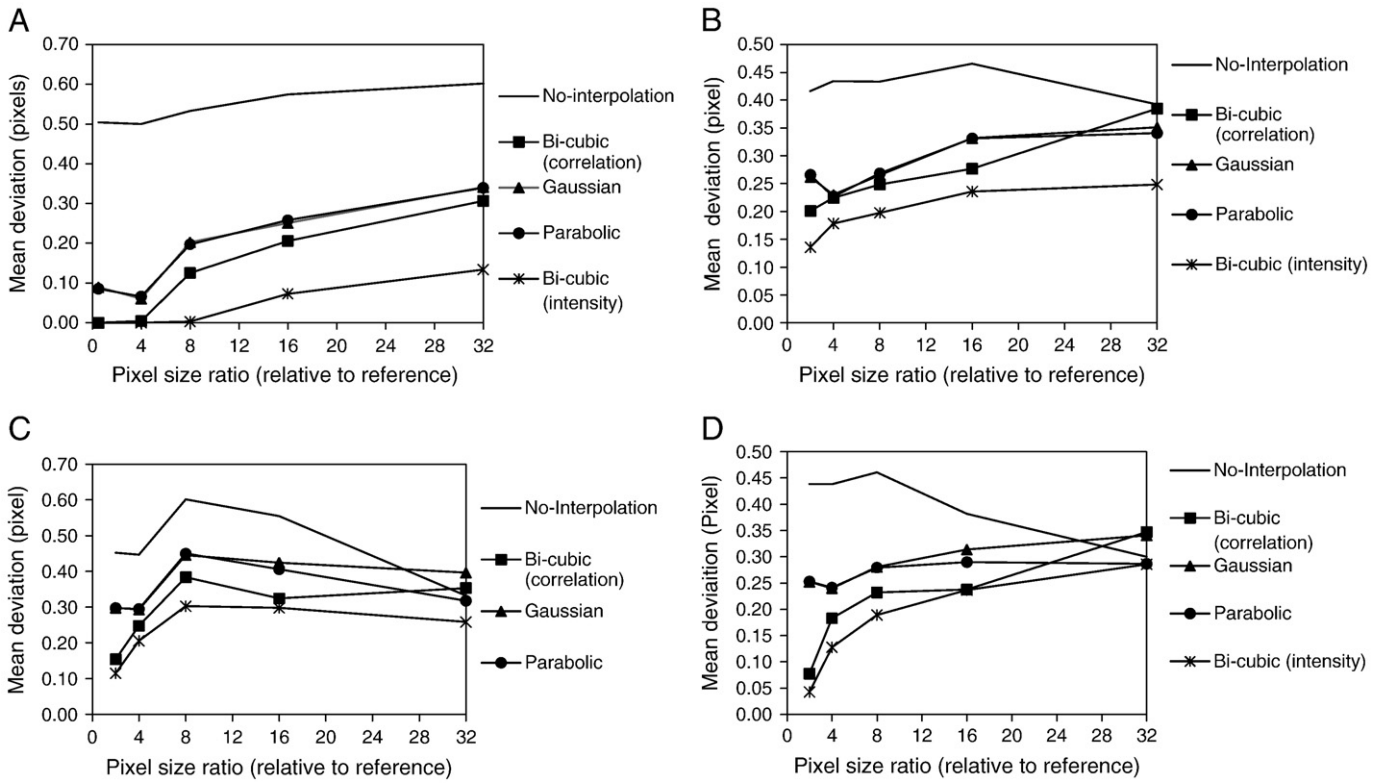

Fig. 11. Mean deviation (normalised to pixel size) of the control set (A), rockglacier (B), landslide (C) and glacier (D) for the different sub-pixel precision algorithms.

much the sub-pixel precision emulates images of the resolution it models. Fig. 12(A) shows that in the case of the control set, intensity interpolation using the bi-cubic convolution can completely (100%) remove the mean deviation between the pixel precision matching position and the high-resolution reference matching position when interpolated up to 1/8th of a pixel. This means for identical but translated images, for instance, when an image of 8 m resolution is used one can use intensity interpolation and compute displacements

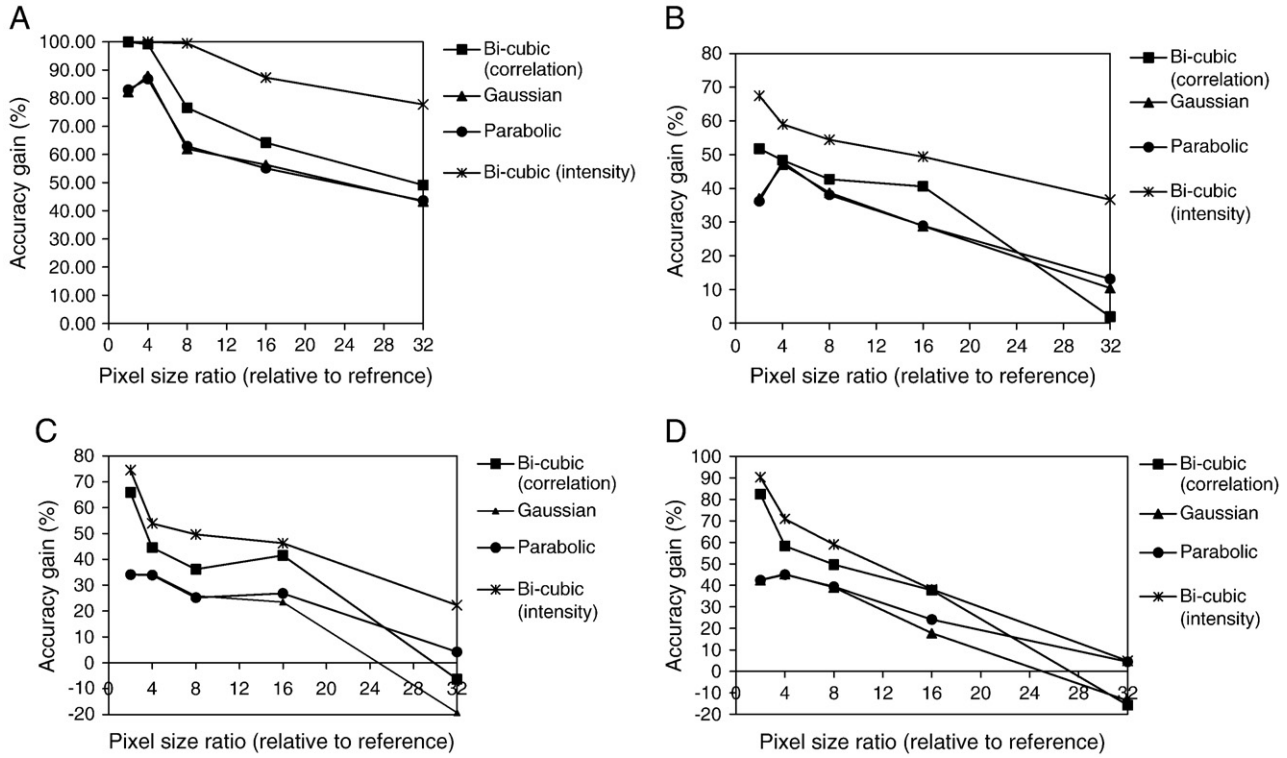

Fig. 12. Percentage accuracy gain in relation to same resolution original image of the control set (A), rockglacier (B), landslide (C) and glacier (D) for the different sub-pixel algorithms.

at 1 m precision and achieve the same accuracy as an original 1 m image. It is important to note that this does not mean that the matching is free of errors. It rather means that the error is the same as the error one would receive if one used original 1 m resolution images. Similar achievements can be obtained using similarity interpolation using bi-cubic interpolation up to only 1/4th of a pixel. Other algorithms could not achieve this 100% removal of the errors; they seem to contain systematic errors.

The algorithms did of course not perform so well for the real mass movements due to the fact that the matched images are not identical. The trends are however the same as the ones found for the control image. Fig. 12(B to D) shows that up to 80% error removal can be achieved. Intensity interpolation performed best in all cases removing in average between 40% and 80% of the mean deviation when interpolated to 1/16th and one half of a pixel, respectively. There is no point of interpolating beyond 1/16th of a pixel as the improvements gained are quite limited. According to our three test cases, for instance when using images of 16 m resolution such as approximately ASTER, one can use intensity interpolation and improve the accuracy of matching by 40% in reference to that obtained from matching 1 m original resolution images, or by 80% in reference to 8 m resolution imagery.

5. Discussion

5.1. Image resolution issues

The effect of the spatial image resolution on the matching accuracy, as presented in Section 4.2, shows that, not surprisingly, all forms of errors increased with increasing pixel size. The mean deviation increased with increasing pixel size simply due to the systematic aggregation of the pixels. The reason why it deviates from linearity for the real mass movements at large pixel sizes can be ascribed to noise due to temporal surface changes, changes in imaging conditions, rotation and deformation which the control set is free of. The control is free of registration errors of the image pairs as well. Additionally and importantly, the fact that the template size is kept constant may have reduced the signal-to-noise ratio due to fewer numbers of pixels per template at large pixel sizes. Real mass movements are more sensitive to this due to the already lower signal-to-noise ratio compared to the control set.

The random error (RMS) increases with pixel size due to a number of reasons. Firstly, for a fixed template size, the number of pixels decreases with increasing pixel size leading to lower information content (lower signal-to-noise ratio). Secondly, the low-resolution images used in this study were created by down-sampling the high-resolution images. Resampling introduces noise which increases with the resampling factor. The introduced noise and the noise that already exists in the original image from various sources lead to a higher RMS and even mismatches. If there are too few pixels in an entity, the entity may get chance-based matches in the target image as ambiguity and noise-related correlation dominates (Kanade & Okutomi, 1991; Westerweel, 1993). In reality, when low-resolution images are used, the random error might not be as high as the ones in this study. Firstly, the template sizes will be adjusted according to the image resolution. Secondly, noise in real images might be lower than that of the comparable resolution images created through down-sampling from high-resolution images.

As both the RMS and the mismatches are results of noise of various sources, image pairs such as the landslide and rockglacier which contain more noise due to the large temporal baselines have more of those errors (Fig. 8B and C). These large periods imply changes of the ground surfaces leading to poorer correlation. The mode of movement of these masses which is far from the pure translation of a rigid body including deformation and rotation also contributes to random errors. Especially the landslide moves in a fragmented pattern lacking good spatial coherence that is needed for good template correlation. The glacier observed over 1 month moves more coherently than the other mass movements and thus shows a relatively lower matching RMS. On the other hand, the control set, which contained only pure translation between otherwise identical images, did not have any random error or mismatch until the pixel size was increased by the factor of 8 and 16 respectively due to reduced signal-to-noise ratio.

The proportion of undetected moving entities increases as the number of entities with displacements less than the pixel size increases (Fig. 8D and Fig. 13). It is obvious that if one continues to increase the pixel size, there will be a point at which no moving template will be detected and the terrain would be reported stable. As can be observed in Fig. 8D, for the specific mass movements investigated here, if only pixel-level precision matching is to be used, the resolution of the images should not be coarser than about 3 m so that the majority of the displacements (less than 3 m) would be detected.

As stated in Section 2, the bi-cubic method of resampling was used for the creation of the resolution pyramid. This does not perform significantly differently from signal averaging that happens within imaging sensors. A test run on the rockglacier image to compare the averaging method and the bi-cubic method showed no observable difference in performance between the two methods except when the factor of down-sampling is high. The difference in performance in the latter case originates from the difference in the number of nearby pixels that contribute to the computation of the value of the resampled pixel in the two methods. While weighted average of the 16 nearest pixels is used for the bi-cubic, arithmetic average of the aggregated pixels is used in the averaging method.

5.2. Performance of the sub-pixel algorithms and levels of detail

Comparison of the sub-pixel precision approaches shows that intensity interpolation outperforms all the other algorithms of similarity interpolation. There can be two explanations to this. Firstly, in correlation interpolation the positions of the correlation values on which the interpolation is based, and which are computed based on coarse resolution images, influence the position of the recomputed correlation peak. Secondly, the number of pixels in an entity is higher when intensity interpolation is applied leading to the suppression of noise. Fewer numbers of pixels in an entity makes the entity more susceptible to chance-based, i.e. erroneous matching results. This is able to explain the increased difference between the performances of the bi-cubic interpolation of the intensity and the correlation surface

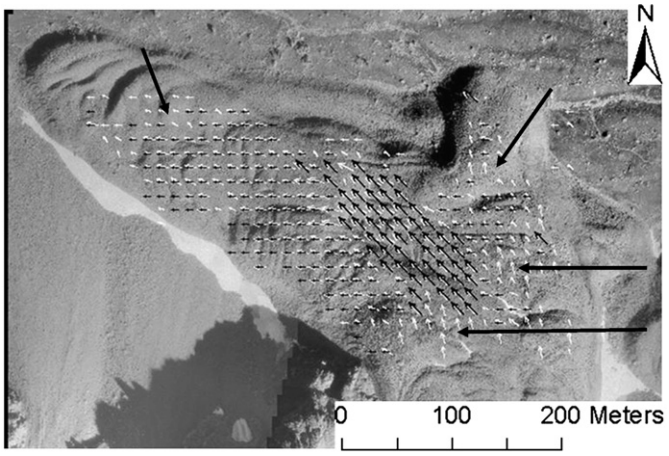

Fig. 13. Spatial variation of the success of image matching at different ground pixel sizes (GPS). Black vectors are computed by matching images of 3.2 m GPS while white vectors are computed by interpolating the images to 0.4 m GPS and matching them afterwards. Notice the slow moving regions indicated by the four thick black arrows.

of the control images at very detailed levels of sub-pixel precision while they are very close at less detail level where the signal-to-noise ratio is still high.

The bi-cubic interpolation scheme that was used for the intensity interpolation is known to replicate the reference data better than most other interpolation schemes (Keys, 1981), and it is known to approximate the *sinc* interpolation that is ideal in image interpolation (Dodgson, 1992). This has led to the fact that the images re-interpolated from coarser resolutions were found to have high correlation with the aerial images of corresponding original resolution. For example, when the down-sampled rockglacier image of resolutions 0.4 m, 0.8 m, 1.6 m, 3.2 m and 6.4 m were re-interpolated to a resolution of 0.2 m (1/2 to 1/32 of a pixel respectively) their global correlation coefficients with the reference image of 0.2 m resolution were 0.98, 0.96, 0.93, 0.90 and 0.86 respectively. Although the images deteriorate due to resampling noise, they still remain well-correlated with the reference image due to the good performance of the interpolation algorithm. Correlation is, in fact, one of the quality measures of image interpolation (Lehmann et al., 1999). Fig. 14 shows a sub-image over rockglacier in the original 0.2 m spatial resolution (A), a 1.6 m spatial resolution image resampled to 0.2 m, i.e. 1/8th, (B) and the 1.6 m spatial resolution itself (C). One can observe the clear image quality of the original 0.2 m spatial resolution (A) as compared to the resampled one (B) which appears to be noisy. The coarse 1.6 m spatial resolution (C) appears blurry showing the lack of detail.

The same interpolation algorithm, bi-cubic, performed also best in the similarity interpolation approach although not as good as in the intensity interpolation. The better performance in comparison to the Gaussian and parabola fitting is partially ascribed to the reasons previously explained. In addition, the parabola fitting is reported in many occasions to have a systematic bias known as “pixel locking”, which forces the estimated sub-pixel locations to approach integer values (Nobach & Honkanen, 2005; Prasad et al., 1992). The presence of a systematic bias is testified by the fact that both parabola and Gaussian fitting could not remove 100% of the errors of pixel-level precision in the case of the control set unlike the other two algorithms (Fig. 12). Although reports from PIV state that Gaussian peak finding does not have that kind of bias and performs better (Westerweel, 1993; Willert & Gharib, 1991), it performed no better than parabola fitting in the present study. We believe the underlying reason is the fact that the cross-correlation surfaces of the mass movements cannot be perfectly modelled by either parabolic or Gaussian functions. The image resolutions used in the present study are not high enough to be compared to that of particle images used in mechanics which are high enough to be approximated by, for example, Gaussian. Noise that is present in the images due to temporal surface changes and other sources contribute to the deviation of the correlation shape from both Gaussian and parabolic ones.

Finally, two important points regarding the size of the matching entities: first, in this study the absolute metric size of the matching entities was kept constant across image resolutions. This means that the number of pixels in each entity varies with the pixel resolution, leading to a variable signal-to-noise ratio. This had to be done for the sake of comparison. In reality, the size of matching entities will vary with the resolution of the image pair to keep a good signal-to-noise ratio. Second, the size of the matching entities was kept constant for the entire scene as is done in most area-based image matching practices.

5.3. Velocity fields

The results of the present study for the Muragl rockglacier correspond very well with those of previous studies (Kääb, 2002; Kääb & Vollmer, 2000). Both the displacement vectors and their spatial variation agree with those studies, although comparison is not the aim here. The maximum velocity recorded here ($0.45\ ma^{-1}$) is only slightly lower than the one recorded by Kääb (2002), i.e. $0.5\ ma^{-1}$, as the latter covered a wider geographical area. This shows the consistency of the NCC as a reliable tool for such applications. Since the Muragl rockglacier creep reflects spatio-temporally variable thermal regimes and ground compositions, also the surface velocities vary. The presented results show mean horizontal velocities over 13 years (1981 to 1994).

Although a number of investigations have been conducted on the dynamics of the great Aletsch Glacier, there are only few regarding the landslides that are occurring in response to the glacier retreat. Investigations made for the period between 1976 and 1995 reported up to 2 m ($10.5\ cm\ a^{-1}$) mean horizontal displacement magnitude (Kääb, 2002, 2005). The 4 m ($13\ cm\ a^{-1}$) maximum horizontal displacement magnitude reported in the present study is for the period 1976 to 2006, and shows only a slight increase in average horizontal velocity.

The displacement and velocity statistics obtained for the Ghiacciaio del Belvedere glacier agree well with the results presented in Kääb et al. (2005). Both studies used the same images. However, since the main focus of the present study was not to investigate the mass movements per se, the full extent of the image was not used. Therefore, the velocities were somewhat overestimated in comparison with the other study as, coincidentally, a part of slow moving areas were left out of the present study. The high velocity of this glacier is recorded also by Haeberli et al. (2002) and Kääb et al. (2004).

The difference in velocity among the three types of masses can be ascribed to the sediment characteristics, terrain type, thermal regime, topography, etc. These velocity differences led to the use of images of different temporal resolutions. Large temporal baselines lead to changes in surface conditions decreasing the potential correlation between the two images. Slow moving masses such as rockglaciers

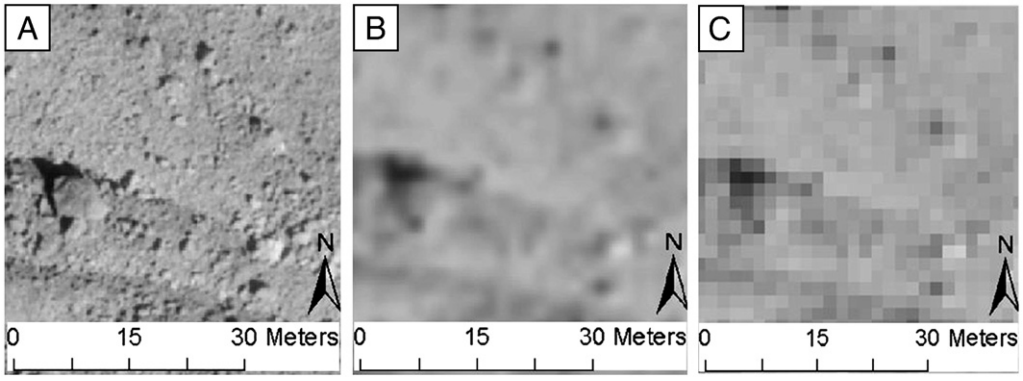

Fig. 14. A part of the Muragl rockglacier image with original 0.2 m spatial resolution (A) and resampled to 0.2 m (B) from a 1.6 m resolution image (C).

and landslides can be investigated using longer temporal baselines. Although the surfaces might not change drastically compared with a glacier, growth of vegetation and erosion of the surface can lead to decorrelation between the two images. This was a challenge in the landslide case. The rockglacier surface was found to be largely stable over the 13 year observation period. This stability owes to the lack of vegetation growth on the rockglacier surface and the somewhat rigid movement due to the geotechnical coherence by ground ice saturation. On the contrary, the landslide moves in a way that is far from rigid-body translation as the rock masses deform and fragment when moving. This leads to poorer correlation, increased random error and even mismatches in cases.

6. Conclusions and outlook

This study has clarified a number of questions around the relation of accuracy and pixel or sub-pixel resolution when matching terrain displacements such as glacier flow, land sliding and permafrost creep from repeat optical images by using pixel-precision correlation measures, here namely the normalised cross-correlation (NCC). The study contributes to better exploiting the large archives of repeat remotely sensed images that exist over actual or potential Earth surface mass movements, as well as to better meeting the increasing needs to quantify and monitor mass movements, in particular when they are accompanied by adverse effects.

The study has in particular evaluated the performance of two different approaches to sub-pixel precision in NCC for displacement measurement based on repeat images. It has also investigated the influence of pixel resolution on image matching and displacement estimation. The findings reveal that with increasing pixel size, all types of matching errors increase. The mean deviation between a displacement and its reference measurement has a linear relationship with the factor by which the pixel size increases. Random errors and mismatches tend to be higher for larger temporal baselines and where the mode of the movement deviates much from rigid-body translation.

When sub-pixel accuracy is aimed for, interpolating image intensities to a higher resolution using bi-cubic interpolation prior to the actual image correlation performs better than both interpolation of the correlation surface using the same algorithm and peak localisation using curve fitting. Correlation peak localisation using the Gaussian and polynomial algorithms are inferior in such applications.

Therefore, we conclude that more precise and accurate displacement measurements are obtained by interpolating the available images to a higher resolution using bi-cubic interpolation prior to matching. In such approaches, one can gain over 40% reduction in mean error (in reference to the same resolution original image) by interpolating the images to up to 1/16th of a pixel. Interpolating to a more detailed sub-pixel resolution than 1/16th of a pixel does not add much. Or in other words, when matching low-resolution images using normalised cross-correlation with intensity-interpolation based sub-pixel precision, 40% or better accuracy increment can be achieved compared to pixel-precision matching in reference to images with the same original resolution as the interpolated image. When actual low-resolution images are used together with varying sizes of matching entities, as opposed to the approach used in this study, even better precision and accuracy might be obtained as the noise due to resampling will not be present, and template and search window sizes will be adjusted with the pixel size.

Although the relative performances of the algorithms is expected to be valid at least for other spatial domain matching approaches and for other applications, the magnitudes given here are strictly valid only for the similarity measure and test sites used in this paper. Validation outside the conditions described in this study requires further research focussing on the development of a rigorous theoretical concept. Future investigations can, for example, aim at comparing the relatively best performing algorithm of this finding to other area-based approaches that intrinsically result in sub-pixel precision, namely least squares matching and Fourier-based phase matching. Besides, the performance of the approach in comparison with feature-based approaches needs to be evaluated as well. There are also other accuracy improving approaches such as pre-processing (e.g. noise filtering) and post-processing (e.g. filtering of displacement vectors by averaging). Further research is needed to know if they even improve the accuracy further after sub-pixel precision.

Acknowledgement

Special thanks are due to three anonymous referees and the editor of the paper for their careful and constructive comments. We would like to express our gratitude to the colleagues of the Geomatics section of our department for their fruitful discussions on the manuscript. We are also very grateful to Kimberly Ann Casey for proof reading of the manuscript. The orthoimages of the Aletsch rockslide and the Muragl rockglacier are based on airphotos acquired by the Swisstopo/flight service (BA057212, BA081844). The orthoimages of the Belvedere glacier are based on airphotos by Swisstopo and CNR-IRPI within the Glaciorisk project. This study is funded by the Research Council of Norway (NFR) through the CORRIA project (no. 185906/V30) and contributes to the NFR International Centre for Geohazards (SFF-ICG 146035/420) and the ESA DUE GlobGlacier project.

References

Althof, R. J., Wind, M. G. J., & Dobbins, J. T., III (1997). A rapid and automatic image registration algorithm with subpixel accuracy. *IEEE Transactions on Medical Imaging*, *16*, 308−316.

Barsch, D. (1996). *Rockglaciers: Indicators for the present and former geoecology in high mountain environments.* Berlin: Springer Verlag.

Brown, L. G. (1992). A survey of image registration techniques. *ACM Computing Surveys*, *24*, 325−376.

Crippen, R. E., & Blom, R. G. (1991). Measurement of subresolution terrain displacements using spot panchromatic imagery. *Geoscience and Remote Sensing Symposium, 1991. IGARSS '91. Remote Sensing: Global Monitoring for Earth Management., International* (pp. 1667−1670).

Delacourt, C., Allemand, P., Casson, B., & Vadon, H. (2004). Velocity field of the "La Clapière" landslide measured by the correlation of aerial and QuickBird satellite images. *Geophysical Research Letters*, *31*, 15−19.

Dodgson, N. A. (1992). *Image resampling.* London: University of Cambridge Computer Laboratory.

Haeberli, W., & Beniston, M. (1998). Climate change and its impacts on glaciers and permafrost in the Alps. *Ambio*, *27*, 258−265.

Haeberli, W., Cihlar, J., & Barry, R. G. (2000). Glacier monitoring within the global climate observing system. *Annals of Glaciology*, *31*, 241−246.

Haeberli, W., Kääb, A., Paul, F., Chiarle, M., Mortara, G., Mazza, A., Deline, P., & Richardson, S. (2002). A surge-type movement at Ghiacciaio del Belvedere and a developing slope instability in the east face of Monte Rosa, Macugnaga, Italian Alps. *Norsk Geografisk Tidsskrift — Norwegian Journal of Geography*, *56*, 104−111.

Haug, T., Kääb, A., & Skvarca, P. (2010). Monitoring ice shelf velocities from repeat MODIS and Landsat data — A method study on the Larsen C ice shelf, Antarctic Peninsula, and 10 other ice shelves around Antarctica. *The Cryosphere*, *4*, 161−178.

Huang, H., Dabiri, D., & Gharib, M. (1997). On errors of digital particle image velocimetry. *Measurement Science and Technology*, *8*, 1427−1440.

Kääb, A. (2002). Monitoring high-mountain terrain deformation from repeated air- and spaceborne optical data: Examples using digital aerial imagery and ASTER data. *ISPRS Journal of Photogrammetry and Remote Sensing*, *57*, 39−52.

Kääb, A. (2005). *Remote sensing of mountain glaciers and permafrost creep.* Zürich: Geographisches Institut der Universität Zürich.

Kääb, A., Huggel, C., Barbero, S., Chiarle, M., Cordola, M., Epifani, F., Haeberli, W., Mortara, G., Semino, P., Tamburini, A., & Viazzo, G. (2004). Glacier hazards at Belvedere Glacier and the Monte Rosa east face, Italian Alps: Processes and mitigation. *Internationales Symposium Interpraevent* (pp. 67−78). Trient: Riva.

Kääb, A., Huggel, C., Fischer, L., Guex, S., Paul, F., Roer, I., Salzmann, N., Schlaefli, S., Schmutz, K., Schneider, D., Strozzi, T., & Weidmann, Y. (2005). Remote sensing of glacier- and permafrost-related hazards in high mountains: An overview. *Natural Hazards and Earth System Sciences*, *5*, 527−554.

Kääb, A., & Vollmer, M. (2000). Surface geometry, thickness changes and flow fields on creeping mountain permafrost: Automatic extraction by digital image analysis. *Permafrost and Periglacial Processes*, *11*, 315−326.

Kanade, T., & Okutomi, M. (1991). A stereo matching algorithm with an adaptive window — Theory and experiment. *1991 IEEE International Conference on Robotics and Automation*, *Vols. 1–3.* (pp. 1088−1095).

Kaufmann, V., & Ladstädter, R. (2003). Quantitative analysis of rock glacier creep by means of digital photogrammetry using multi-temporal aerial photographs: Two case studies in the Austrian Alps. In M. Phillips, S. M. Springman, & L. U. Arenson

(Eds.), *Eighth international conference on permafrost* (pp. 525—530). Zurich, Switzerland: Taylor & Francis.
Keys, R. G. (1981). Cubic convolution interpolation for digital image processing. *IEEE Transactions on Acoustics, Speech, and Signal Processing*, *29*, 1153—1160.
Lehmann, T. M., Gonner, C., & Spitzer, K. (1999). Survey: Interpolation methods in medical image processing. *IEEE Transactions on Medical Imaging*, *18*, 1049—1075.
Leprince, S., Barbot, S., Ayoub, F., & Avouac, J. P. (2007). Automatic and precise orthorectification, coregistration, and subpixel correlation of satellite images, application to ground deformation measurements. *IEEE Transactions on Geoscience and Remote Sensing*, *45*, 1529—1558.
Lewis, J. P. (1995). Fast normalized cross-correlation. *Vision Interface*, 120—123.
Lourenco, L., & Krothapalli, A. (1995). On the accuracy of velocity and vorticity measurements with PIV. *Experiments in Fluids*, *18*, 421—428.
Meijering, E., & Unser, M. (2003). A note on cubic convolution interpolation. *IEEE Transactions on Image Processing*, *12*, 477—479.
Nobach, H., & Honkanen, M. (2005). Two-dimensional Gaussian regression for sub-pixel displacement estimation in particle image velocimetry or particle position estimation in particle tracking velocimetry. *Experiments in Fluids*, *38*, 511—515.
Prasad, A., Adrian, R., Landreth, C., & Offutt, P. (1992). Effect of resolution on the speed and accuracy of particle image velocimetry interrogation. *Experiments in Fluids*, *13*, 105—116.
Quincey, D. J., Lucas, R. M., Richardson, S. D., Glasser, N. F., Hambrey, M. J., & Reynolds, J. M. (2005). Optical remote sensing techniques in high-mountain environments: Application to glacial hazards. *Progress in Physical Geography*, *29*, 475—505.
Rebetez, M., Lugon, R., & Baeriswyl, P. -A. (1997). Climatic change and debris flows in high mountain regions: The case study of the Ritigraben Torrent (Swiss Alps). *Climatic Change*, *36*, 371—389.
Ritter, M. (2006). *The physical environment: an introduction to physical geography*. 10.01.2009: http://www.uwsp.edu/geo/faculty/ritter/geog101/textbook/title_page.html, 14.06.2010.
Scambos, T. A., Dutkiewicz, M. J., Wilson, J. C., & Bindschadler, R. A. (1992). Application of image cross-correlation to the measurement of glacier velocity using satellite image data. *Remote Sensing of Environment*, *42*, 177—186.
Scherler, D., Leprince, S., & Striker, M. R. (2008). Glacier-surface velocities in alpine terrain from optical satellite imagery–accuracy improvement and quality assessment. *Remote Sensing of Environment*, *112*, 3806—3819.
Shimizu, M., & Okutomi, M. (2002). An analysis of sub-pixel estimation error on area-based image matching. *14th International Conference on Digital Signal Processing* (pp. 1239—1242).
Skvarca, P., Arup, B., & De Angelis, H. (2003). Recent behaviour of Glaciar Upsala, a fast-flowing calving glacier in Lago Argentino, southern Patagonia. *Annals of Glaciology*, *36*, 184—188.
Szeliski, R., & Scharstein, D. (2002). Symmetric sub-pixel stereo matching. *Computer Vision — ECCV 2002* (pp. 657—659).
Taylor, M. H., Leprince, S., Avouac, J. P., & Sieh, K. (2008). Detecting co-seismic displacements in glaciated regions: An example from the great November 2002 Denali earthquake using SPOT horizontal offsets. *Earth and Planetary Science Letters*, *270*, 209—220.
Toutin, T. (2004). Review article: Geometric processing of remote sensing images: models, algorithms and methods. *International Journal of Remote Sensing*, *25*, 1893—1924.
Vosselman, G., Sester, M., & Mayer, H. (2004). Basic computer vision techniques. In J. C. McGlone (Ed.), *Manual of photogrammetry* (pp. 455—504). Bethesda: American Society of Photogrammetry and Remote Sensing.
Wangensteen, B., Gumundsson, Á., Eiken, T., Kääb, A., Farbrot, H., & Etzelmüller, B. (2006). Surface displacements and surface age estimates for creeping slope landforms in Northern and Eastern Iceland using digital photogrammetry. *Geomorphology*, *80*, 59—79.
Westerweel, J. (1993). *Digital particle image velocimetry: Theory and application.* Delft: Delft University Press.
Whillans, I. M., & Tseng, Y. -H. (1995). Automatic tracking of crevasses on satellite images. *Cold Regions Science and Technology*, *23*, 201—214.
Willert, C. E., & Gharib, M. (1991). Digital particle image velocimetry. *Experiments in Fluids*, *10*, 181—193.
Yamaguchi, Y., Tanaka, S., Odajima, T., Kamai, T., & Tsuchida, S. (2003). Detection of a landslide movement as geometric misregistration in image matching of SPOT HRV data of two different dates. *International Journal of Remote Sensing*, *24*, 3523—3534.
Zhao, F., Huang, Q. M., & Gao, W. (2006). Image matching by normalized cross-correlation. *31st IEEE International Conference on Acoustics, Speech and Signal Processing* (pp. 1977—1980). Centre de Congrès Pierre Baudis Toulouse, France.
Zitová, B., & Flusser, J. (2003). Image registration methods: A survey. *Image and Vision Computing*, *21*, 977—1000.